Flowfield Calculation of Electrothermal Pulsed Plasma Thrusters for the PROITERES Satellite

IEPC-2011-037

Presented at the 32nd International Electric Propulsion Conference,
Wiesbaden • Germany
September 11 – 15, 2011

Hirokazu Tahara[1],Yusuke Ishii[2], Masato Tanaka[3] and Masamichi Naka[4]
Osaka Institute of Technology
Asahi-Ku, Osaka, 535-8585, Japan

and

Yosuke Watanabe[5]
Osaka University
Toyonaka, Osaka 560-8531, Japan

Abstract: The Project of Osaka Institute of Technology Electric-Rocket-Engine onboard Small Space Ship (PROITERES) was started at Osaka Institute of Technology in 2007. In PROITERES, a nano-satellite with electrothermal pulsed plasma thrusters (PPTs) will be launched in 2012, because the launching was delayed due to change of schedule of Indian PSLV launcher. The main mission is powered flight of nano-satellite by electric thruster. An unsteady numerical simulation was carried out to investigate physical phenomena in the discharge system including plasma and discharge electric circuit and to predict performance characteristics for electrothermal PPTs. The calculated Mach number intensively increased downstream from the discharge cavity exit; that is, the supersonic flow was established in the nozzle cathode. Both the calculated impulse bit and mass shot agreed well with the measured ones. The calculated results of 40,000-shot endurance test also agreed with the measured ones. Furthermore, the research and development of the 2nd PROITERES satellite with high-power and large-total-impulse PPT system are also introduced.

Nomenclature

C	=	electric capacitance
e	=	internal energy or electron charge
E_i	=	corresponding voltage of ionization
j	=	current density
J	=	discharge current
k	=	Boltzmann factor or heat conductivity
L	=	electric inductance
m	=	particle mass
M	=	momentum flux

[1] Professor, Department of Mechanical Engineering, and tahara@med.oit.ac.jp.
[2] Graduate Student, Department of Mechanical Engineering, and tahara@med.oit.ac.jp.
[3] Graduate Student, Department of Mechanical Engineering, and tahara@med.oit.ac.jp.
[4] Graduate Student, Department of Mechanical Engineering, and tahara@med.oit.ac.jp.
[5] Research Associate, Graduate School of Engineering Science, and watanabe@me.es.osaka-u.ac.jp.

n = number density
p = pressure
q = heat flux
Q = Joule heat
r = radial coordinate
R = electric resistance
t = time
T = temperature
V = velocity
z = axial coordinate
α = degree of ionization
φ = particle number flux
ρ = density
ρ_p = electric resistance
$\sigma_{e\text{-}n}$ = cross-section of electron-neutral collision
Γ = mass flux
Θ = temperature
$ln\Lambda$ = Coulomb logarithm

Subscript

0 = initial
e = electron
i = ion
n = neutral
r = radial direction
s = surface
z = axial direction

I. Introduction

THE Project of Osaka Institute of Technology Electric-Rocket-Engine onboard Small Space Ship (PROITERES), as shown in Fig.1, was started at Osaka Institute of Technology.[1,2] In PROITERES, a small satellite with electrothermal pulsed plasma thrusters (PPTs) will be launched in 2012, because the launching was delayed from the end of 2011 due to change of schedule of Indian PSLV launcher. The main mission is powered flight of nano satellite by electric thruster. The orbit raising will be carried out by the PPTs.

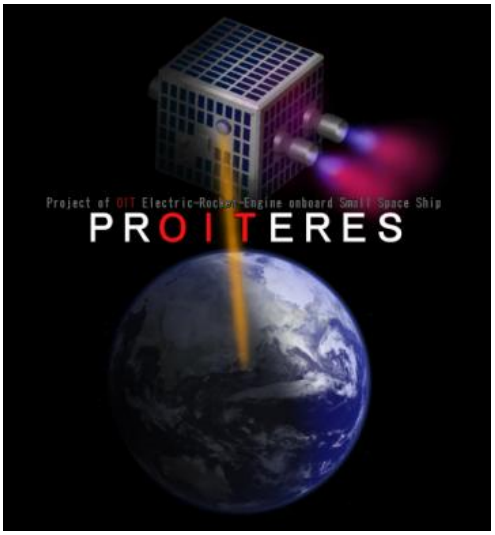

Figure 1. Illustration of powered flight of Osaka Institute of Technology small space ship by electric rocket engine.

Pulsed plasma thrusters are expected to be used as thrusters for small/nano satellites. The PPT has some features superior to other kinds of electric propulsion. It has no sealing part, simple structure and high reliability, which are benefits of using a solid propellant, mainly Teflon® (poly-tetrafluoroethylene: PTFE). However, performances of PPTs are generally low compared with other electric thrusters.[3-12]

At Osaka Institute of Technology, the PPT has been studied since 2003 in order to understand physical phenomena and improve thrust performances with both experiments and numerical simulations. We mainly studied electrothermal-acceleration-type PPTs, which generally had higher thrust-to-power ratios (impulse bit per unit initial energy stored in capacitors) and higher thrust efficiencies than electromagnetic-acceleration-type PPTs. Although the electrothermal PPT has lower specific impulse than the electromagnetic PPT, the low specific impulse is not a significant problem as long as the PPT uses solid propellant, because there is no tank nor valve for liquid or gas propellant which would be a large weight proportion of a thruster system.

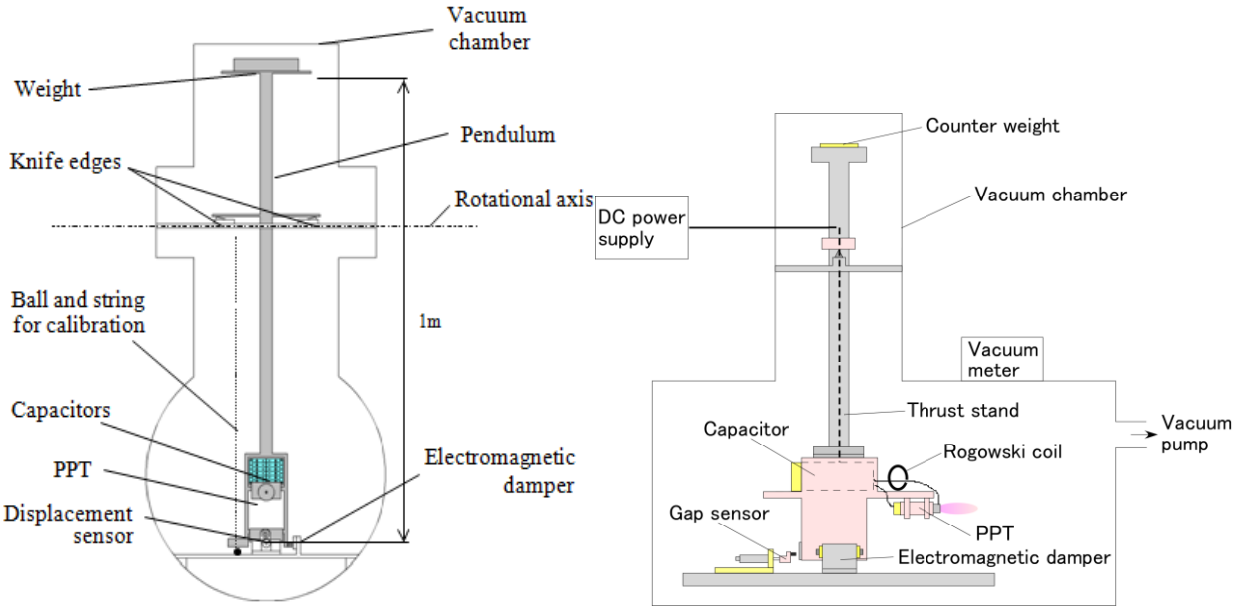

Figure 2. Thrust stand installed in vacuum chamber.

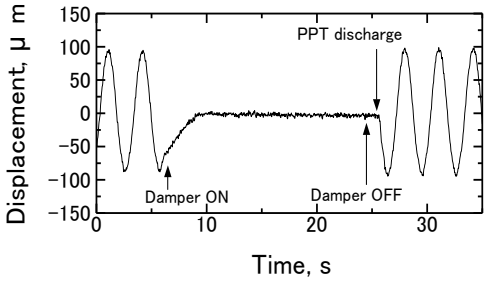

Figure 3. Typical signal of displacement in a measurement of impulse bit.

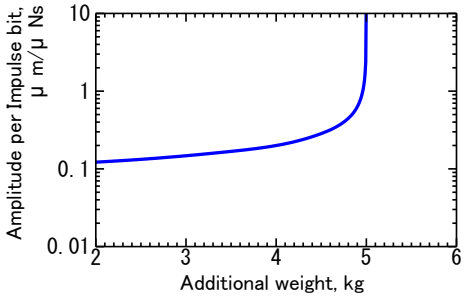

Figure 4. Sensitiveness of thrust stand vs top weight.

Figure 5. Vacuum chamber.

In the present study, an unsteady numerical simulation is carried out to examine physical phenomena in the PPT discharge system including plasma and discharge electric circuit and to predict performance characteristics for small/nano satellites like PROITERES. Furthermore, the research and development of the 2nd PROITERES satellite with high-power and large-total-impulse PPT system are also introduced.

II. Thrust Measurement System

Figure 2 shows a thrust stand in a vacuum chamber for precise measurement of an impulse bit. The PPT and capacitors are mounted on the pendulum, which rotates around fulcrums of two knife edges without friction. The displacement of the pendulum is detected by an eddy-current-type gap sensor (non-contacting micro-displacement meter) near the PPT, which resolution is about ±0.5 μm. The electromagnetic damper is used to suppress mechanical noises and to decrease quickly the amplitude for the next measurement after firing the PPT. It is useful for a sensitive thrust stand because it is non-contacting. The damper consists of a permanent magnet fixed to the pendulum and two coils fixed to the supporting stand. The control circuit differentiates the output voltage of the displacement sensor and supplies the current proportional to the differentiated voltage to the coil. Accordingly, the damper works as a viscosity resistor. The damper is turned off just before firing the PPT for measurements without damping, and turned on after the measurement to prepare for

the next measurement. Figure 3 shows a typical signal of displacement in measurement of impulse bit. Sensitiveness of the thrust stand is variable by changing the weight mounted on the top of the pendulum as shown in Fig. 4. A calibration of the thrust stand is carried out by collisions of balls with various masses to the pendulum from various distances corresponding 15-1400 μNs.

Figure 5 shows a vacuum chamber 1.25 m in length and 0.6 m in inner diameter, which is evacuated using a turbo-molecular pump with a pumping speed of 3,000 l/s. The pressure is kept below 1.0×10^{-2} Pa during PPT operation.

III. Numerical Calculation

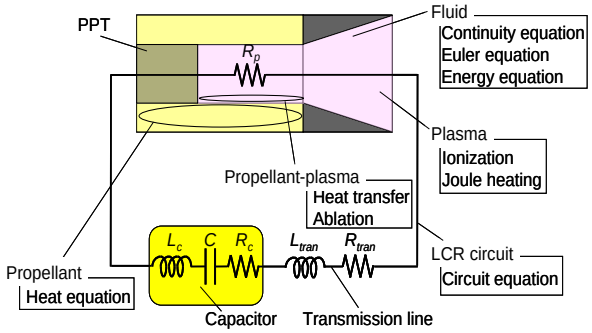

Figure 6. Calculation model for PPT system.

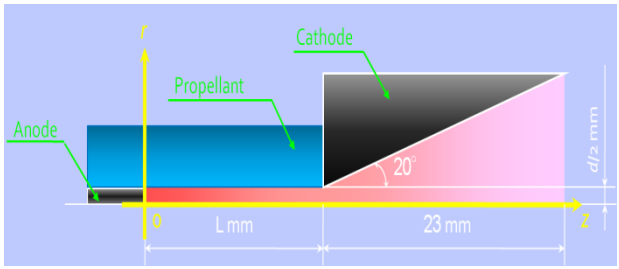

Figure 7. Calculation domain

A. Calculation Model

An unsteady numerical simulation is carried out to investigate physical phenomena in the PPT discharge system including plasma and discharge electric circuit and to predict performance characteristics.[9-15] Figure 6 shows the calculation model of the PPT system. The calculation simultaneously simulates unsteady phenomena of discharge in the circuit, heat transfer to the PTFE, heat conduction inside the PTFE, ablation from the PTFE surface and plasma flow. The calculation domain of the discharge chamber, as shown in Fig. 7, in the nozzle cathode and in the cylindrical cavity made of PTFE (Teflon). The length and diameter of the cavity are changed considering operational conditions.

B. Governing Equations

Axisymmetric two-dimensional unsteady flowfield equations, conservation equations of mass, momentum and energy, are written as follows:

Mass:

$$\frac{\partial}{\partial t}\rho + \frac{\partial}{\partial r}M_r + \frac{\partial}{\partial z}M_z = -\frac{1}{r}M_r \tag{1}$$

Momentum (Euler Eqs.):

r-direction:

$$\frac{\partial}{\partial t}M_r + \frac{\partial}{\partial r}\left[\frac{M_r^{\,2}}{\rho} + p\right] + \frac{\partial}{\partial z}\left[\frac{M_r M_z}{\rho}\right] = -\frac{1}{r}\frac{M_r^{\,2}}{\rho} \tag{2}$$

z-direction:

$$\frac{\partial}{\partial t}M_z + \frac{\partial}{\partial r}\left[\frac{M_r M_z}{\rho}\right] + \frac{\partial}{\partial z}\left[\frac{M_z^{\,2}}{\rho} + p\right] = -\frac{1}{r}\frac{M_r M_z}{\rho} \tag{3}$$

Energy:

$$\frac{\partial}{\partial t}e + \frac{\partial}{\partial r}\left[\frac{M_r}{\rho}(e+p)\right] + \frac{\partial}{\partial z}\left[\frac{M_z}{\rho}(e+p)\right] = -\frac{1}{r}\frac{M_r}{\rho}(e+p) + Q_j \tag{4}$$

where ρ, p, and e are density, pressure and internal energy of flow, respectively, and M_r and M_z are momentum fluxes of raidial and axial directions, respectively. Q_j is Joule heat.

Ionization equilibrium is assumed as follows:

Saha Eq.:

$$\frac{\alpha^2}{1-\alpha^2} = 2.6\frac{(kT)^{5/2}(2\pi m_e)^{3/2}}{p\,h^3}\exp\left(-\frac{qE_i}{kT}\right) \tag{5}$$

where α and T are degree of ionization and temperature of flow, respectively, and E_i is corresponding voltage of ionization, in which the average ionization voltage of PTFE decomposed atoms (carbon and hydrogen etc.) are used.

The Joule heat is written as follows:

$$Q_j = \rho_p\, j^2 \tag{6}$$

$$\rho_p = \frac{\ln \Lambda}{1.53\times10^{-2}T^{3/2}} + \frac{m_e}{n_e e^2}\cdot\sigma_{e-n}n_n\left(\frac{3kT}{m_e}\right)^{1/2}$$

$$\ln\Lambda = \ln[12\pi n_e(\varepsilon_0 kT/e^2 n_e)^{3/2}]$$

where ρ_p is electric resistance corresponding electron-ion and electron-neutral collisions, in which n_e and n_n are densities of electron and neutral, respectively, and j is current density in axial direction.

Figure 8 shows the model of heat fluxes from plasma to PTFE surface in the cavity, and their heat fluxes and the interaction are written as follows:

Heat convection:

$$q_{h,conv} = a_i(\varphi_i + \varphi_n)\cdot 2k(T_{h,w} - T_s) \tag{7}$$

Heat conduction:

$$q_{h,cond} = k\frac{\partial T_{h,w}}{\partial r} \tag{8}$$

Interaction Eq.:

$$q_{h,conv} = q_{h,cond} \tag{9}$$

where φ_i and φ_n are particle number fluxes of ion and neutral, respectively, to PTFE surface.

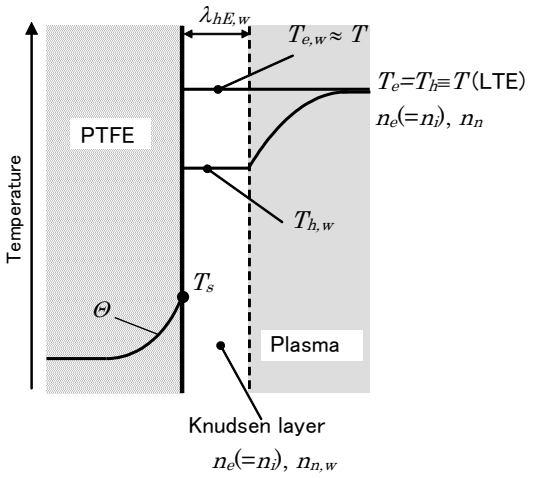

Figure 8. Heat transfer inside PTFE.

In evaporation of PTFE on the cavity wall, we use the following equations:

Langmuir's law:

$$\Gamma = \left(\frac{m_n}{2\pi kT_s}\right)^{1/2} p_{vap} \tag{10}$$

$$p_{vap} = p_c \exp(-T_c/T_s)$$

(p_c = 1.84 × 1015 Pa、T_c = 20815 K)

Evaporation heat flux:

$$q_{ab} = \frac{\Gamma}{m_n}\cdot 2kT_s \tag{11}$$

where Γ and q_{ab} are mass and heat fluxes, respectively, from PTFE surface, and p_{va} and T_s are evaporation pressure and PTFE surface temperature, respectively.

In heat conduction inside the PTFE block, the heat conduction equation and the boundary condition are written as follows:

$$\frac{\partial\Theta}{\partial t} = \frac{\kappa}{\rho_{PTFE}C_p}\left(\frac{\partial^2\Theta}{\partial r'^2} + \frac{1}{r'}\frac{\partial\Theta}{\partial r'} + \frac{\partial^2\Theta}{\partial z^2}\right) \tag{12}$$

$$\kappa\left.\frac{\partial\Theta}{\partial r}\right|_{r=0} = (Q_{conv} - Q_{ab})$$

where Θ is temperature inside the PTFE.

Finally, we close the equation system by using the following electric circuit equation:

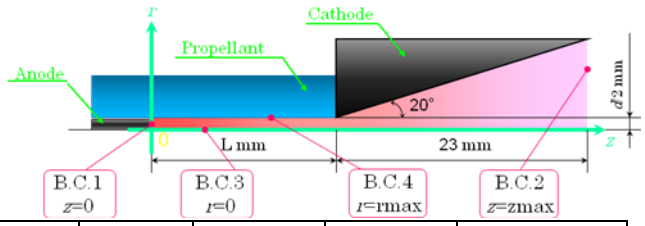

	ρ	M_r	M_z	e
B.C 1	$\frac{\partial \rho}{\partial z}=0$	$\frac{\partial M_r}{\partial z}=0$	$M_z=0$	$\frac{\partial e}{\partial z}=0$
B.C 2	$\frac{\partial \rho}{\partial z}=0$	$\frac{\partial M_r}{\partial z}=0$	$\frac{\partial M_z}{\partial z}=0$	$\frac{\partial e}{\partial z}=0$
B.C 3	$\frac{\partial \rho}{\partial r}=0$	$M_r=0$	$\frac{\partial M_z}{\partial r}=0$	$\frac{\partial e}{\partial r}=0$
B.C 4	$\Delta\rho_r=\rho_{ab}$	$M_r=\Gamma$	$\frac{\partial M_z}{\partial r}=0$	$\Delta e_r=Q_{ab}-Q_{conv}$

Figure 9. Boundary conditions.

From Fig. 6:

$$(L_{tran}+L_c)\ddot{Q}+(R_{tran}+R_c+R_p)\dot{Q}+\frac{Q}{C}=0 \quad (13)$$

$$J=-\dot{Q}$$

Initial condition:

$$Q_0=CV_0$$

Table 1. Experimental and calculating condition with discharge energy per one shot of 14.6 J/s.

Discharge chamber	Length, mm	19
	Diameter, mm	2.5, 3.0, 3.5
Nozzle	Length, mm	23
	Half angle, degree	20
Charging voltage, V		1800
Capacitance, μF		9.0

Table 2. Experimental and calculating condition with discharge energy per one shot of 2.4 J/s.

Discharge chamber	Length, mm	9.0
	Diameter, mm	1.0, 1.5, 2.0, 2.5
Nozzle	Length, mm	23
	Half angle, degree	20
Charging voltage, V		1800
Capacitance, μF		1.5

Table 3. Experimental and calculating conditionof endurance test

Discharge chamber	Length, mm	10.0
	Diameter, mm	1.0
Nozzle	Length, mm	23
	Half angle, degree	20
Capacitance, μF		1.5
Charging voltage, V		1800
Inductance, μH		0.35
Resistance, Ω		0.05

C. Calculation Procedure and Conditions

After all equations were normalized, the flowfield equations are numerically solved by TVD-MacCormack scheme and average of Roe. In the calculation process, the electric circuit equation is solved by Runge-Kutta method, and the axial current density is obtained. The boundary conditions shown in Fig. 9 are assumed. For calculation start, a very low density plasma is distributed just before the calculation. The calculation grid sizes are 0.5 mm in axial direction and 0.025 mm in radial direction, and the time step is 10^{-9} s.

The experimental and calculation conditions are shown in Tables 1 and 2. The discharge energies per one shot are 14.6 and 2.4 J/shot; that is, the capacitance is changed. Accordingly, the length and diameter of discharge cavity are changed to find preferable cavity configuration. The discharge energy per one shot is lowered to 2.4 J/shot for the nano satellite. The experimental and calculation conditions are also shown in Table 3.

IV. Results and Discussion

A. Calculation Results

Figure 10 shows typical measured and calculated discharge current waveformss with a discharge energy of 14.6 J/s. The calculated current signal agrees with the measured one.

Figure 11 shows the calculated Mach number distribution just after 3 μs from the discharge start with 14.6 J/s. The Mach number intensively increases downstream from z=19mm; that is, the supersonic flow is established. At z=35mm, the Mach number drastically decreases downstream, resulting from structure of shock wave.

Figure 12 shows the calculated time histories of normalized density, thrust, ablated mass and Joule heating at r=1.25mm and z=9.5mm with 14.6 J/s. The Joule heating begins at approximately 1 μs; it is completed by 7 μs, and the ablation from the PTFE surface relays about 1-2 μs from the Joule heating. The density gradually increases from about 2 μs; it has a peak at 9 μs, and then it decreases. The thrust gradually increases from 4 μs, and it has a peak at

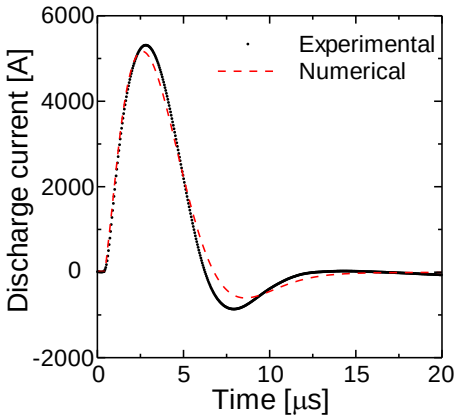

Figure 10. Discharge current waveform.

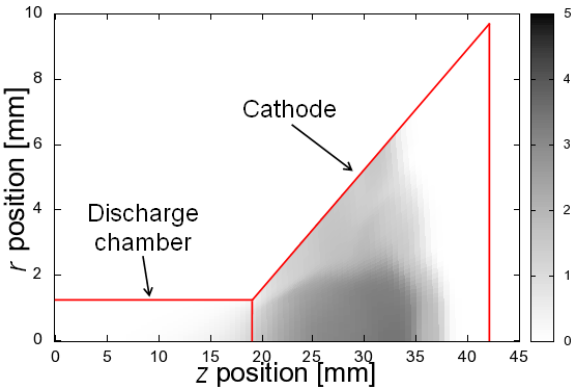

Figure 11. Mach number distribution.

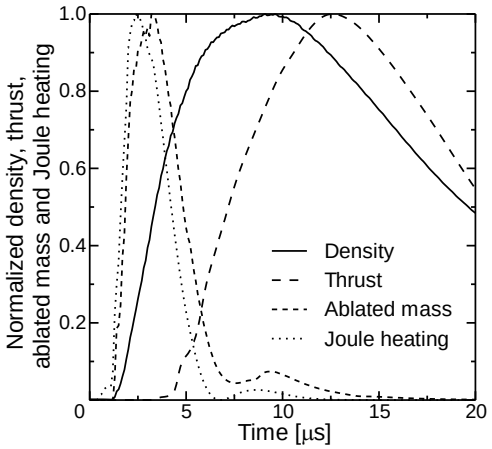

Figure 12. Normalized density, thrust, Joule heating and ablated mass.

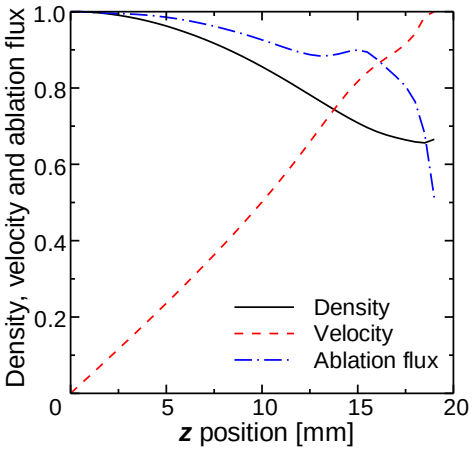

Figure 13. Normalized density, velocity and ablation flux.

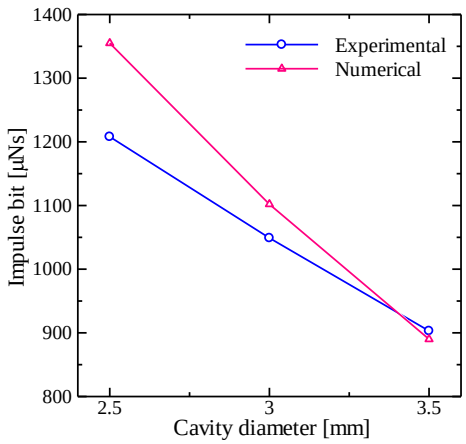

a)

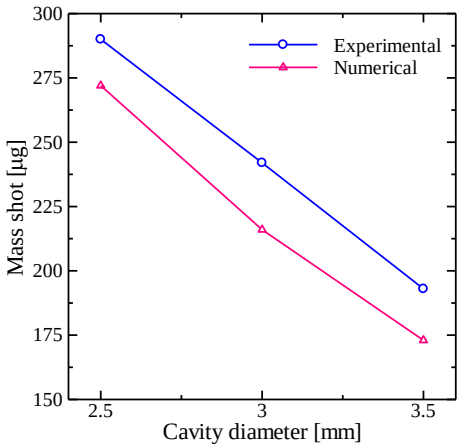

b)

Figure 14. Experimental and numerical results with discharge energy per one shot of 14.6 J/s. a) Impulse bit, b) mass shot.

13 μs. Accordingly, the thrust is generated until over 20 μs. Thrust generation is expected to be related to increase in density.

Figure 13 shows axial the calculated distributions of normalized density, velocity and ablation flux near the cavity wall just after 10 μs from the discharge start with 14.6 J/s. The velocity linearly increases from the upstream

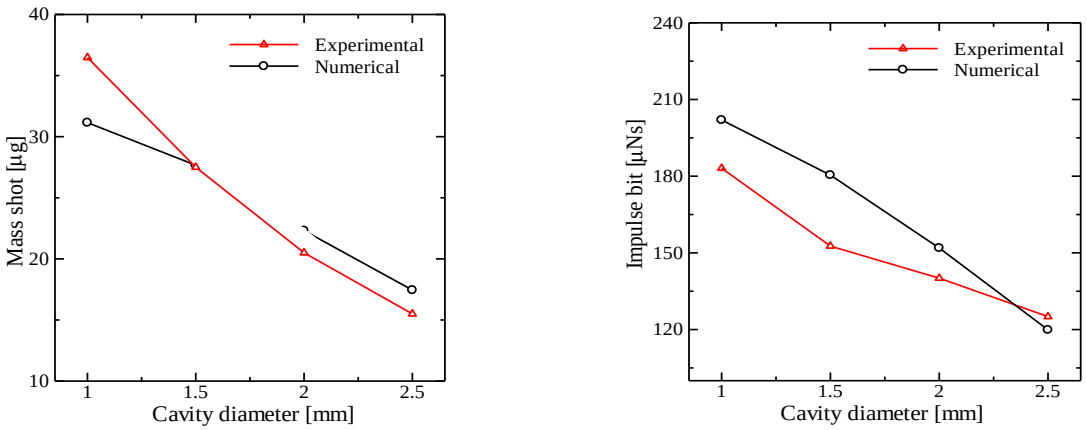

a) **b)**

Figure 15. Experimental and numerical results with discharge energy per one shot of 2.4 J/s. a) Impulse bit, b) mass shot.

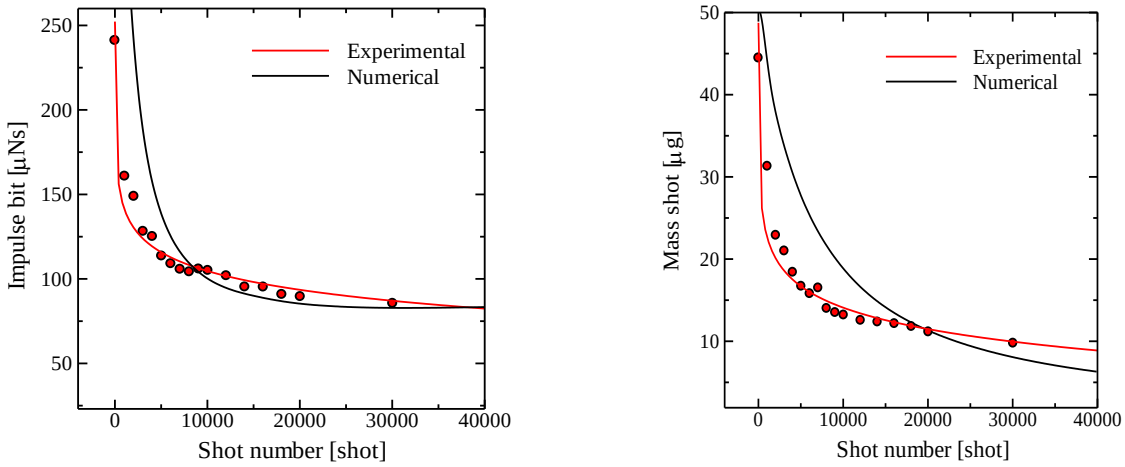

a) **b)**

Figure 16. Experimental and numerical results of endurance test with 2.4 J/s. a) Impulse bit, b) mass shot.

end to the cavity exit although the density gradually decreases. An axial decrease in ablation flux is due to the axial decrease in density because of lowering heat convection to the PTFE surface.

B. Comparisons with Experimental Results

Figure 14 shows measured and calculated impulse bit and mass shot dependent on cavity diameter with a constant cavity length of 19 mm with a discharge energy per one shot of 14.6 J/s. Both the impulse bit and the mass shot decrease with increasing cavity diameter regardless of calculation and experiment. The calculated impulse bit roughly agrees with the measured one although with a small diameter of 2.5 mm it is slightly higher. On the other hand, the calculated mass shot agrees with the measured one, and its error is within 10 % although it is lower with all cavity diameters.

Figure 15 shows measured and calculated impulse bit and mass shot dependent on cavity diameter with a constant cavity length of 9 mm with a discharge energy per one shot of 2.4 J/s. Both the calculated impulse bit and mass shot agreed with the measured ones even with low discharge energies.

C. Calculated Endurance Test Results

We simply calculated repetitive operation modes, i.e., endurance tests of the PPT system by using an one-dimensional model with the same assumptions of the axisymmetric model. Figure 16 shows the calculated results.

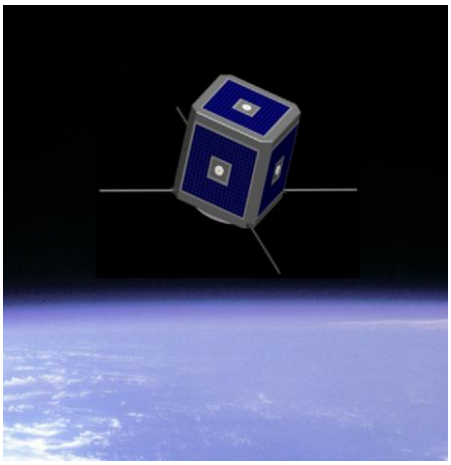

Figure 17. Illustration of 2nd PROITERES satellite.

Both the impulse bit and the mass shot have the maximum errors of 25 % compared with the measured ones in the range up to 20,000 shots. However, they agree well with the measured ones in the long operation above 20,000 shots.

V. 2nd PROITERES Satellite R&D

As next projects, we started the research and development of the 2nd PROITERES satellite in Oct. 2010. The 2nd satellite of PROITERES series, as illustrated in Fig.17, is a 50-kg earth-observation satellite with high-power and large-total-impulse pulsed plasma thruster system for practical use. The PPT system with 10-15 kg is provided with four thruster heads with Teflon feeding mechanisms, and the total impulse per one thruster head is 2500 Ns at an input power of 25 W. As a result, we can change totally the altitude of the satellite up to 400 km, and on the lower orbit of 200 km we can keep the altitude up to one month. The 2nd PROITERES satellite is under development and under accurate prediction of PPT performance.

VI. Conclusion

An unsteady numerical simulation was carried out to investigate physical phenomena in the PPT discharge system including plasma and discharge electric circuit and to predict performance characteristics for small/nano satellites like PROITERES satellites.

The Mach number intensively increased downstream from z=19mm of the discharge cavity exit; that is, the supersonic flow was established. At z=35mm in the nozzle cathode, the Mach number drastically decreased downstream, resulting from structure of shock wave.

In a discharge cavity, the Joule heating and the ablation from the PTFE surface were completed up to 10 μs just after the discharge start. After the intensive ablation, the thrust was generated until over 20 μs. The velocity linearly increased from the upstream end to the discharge cavity exit although the density gradually decreased. An axial decrease in ablation flux was due to the axial decrease in density.

With a discharge energy per one shot of 14.6 J/s, both the impulse bit and the mass shot decreased with increasing cavity diameter regardless of calculation and experiment. The calculated impulse bit roughly agreed with the measured one. On the other hand, the calculated mass shot agreed well with the measured one. In a case with a low energy of 2.4 J/s, both the calculated impulse bit and mass shot agreed with the measured ones.

In calculated repetitive operation modes, i.e., endurance tests of the PPT system by using the one-dimensional model, both the impulse bit and the mass shot had the maximum errors of 25 % compared with the measured ones in the range up to 20,000 shots. However, they agreed well with the measured ones in the long operation above 20,000 shots.

Consequently, the simulation code can be completely accepted to roughly predict performance of PPT systems for small/nano satellites.

As next projects, we started the research and development of the 2nd PROITERES satellites in Oct. 2010. The 2nd satellite of PROITERES series is a 50-kg earth-observation satellite with high-power and large-total-impulse pulsed plasma thruster system for practical use. The PPT system with 10-15 kg is provided with four thruster heads with Teflon feeding mechanisms, and the total impulse per one thruster head is 2500 Ns at an input power of 25 W. The 2nd PROITERES satellite is under development and under accurate prediction of PPT performance.

References

[1]Yamada, M., and Tahara, H.," Progress of Project of Osaka Institute of Technology Electric-Rocket-Engine onboard Small Space Ship," *27th International Symposium on Space Technology and Science*, Paper ISTS 2009-s-05f, 2009.

[2]Ozaki, J., Ikeda, T., Fujiwara, T., Nishizawa, M., Araki, S., Tahara, H., and Watanabe, Y.," Development of Osaka Institute of Technology Nano-Satellite "PROITERES" with Electrothermal Pulsed Plasma Thrusters," *32nd International Electric Propulsion Conference*, Paper No. IEPC-2011-035, Wiesbaden, Germany, 2011.

[3]Naka, M., Hosotani, R., Tahara, H., and Watanabe, Y.," Development of Electrothermal Pulsed Plasma Thruster System Flight-Model for the PROITERES Satellite," *32nd International Electric Propulsion Conference*, Paper No. IEPC-2011-034, Wiesbaden, Germany, 2011.

[4]Burton, R. L., and Turchi, P. J.," Pulsed Plasma Thruster," *Journal of Propulsion and Power*, Vol.14, No.5, 1998, pp.716-735.

[5]Edamitsu, T., Tahara, H., and Yoshikawa, T.," Performance Characteristics of a Coaxial Pulsed Plasma Thruster with PTFE Cavity," *Proc. Asian Joint Conferences on Propulsion and Power 2004*, 2004, pp.324-334.

[6]Edamitsu, T., Tahara, H., and Yoshikawa, T.," Effects of Cavity Length and Material on Performance Characteristics of a Coaxial Pulsed Plasma Thruster," *24th International Symposium on Space Technology and Science*, Paper ISTS-2004-b-6, 2004.

[7]Rysanek, F., and Burton, R. L.," Performance and Heat Loss of a Coaxial Teflon Pulsed Thruster," *27th International Electric Propulsion Conference*, Paper IEPC-01-151, 2001.

[8]Burton, R. L., Wilson, M. J., and Bushman, S. S.," Energy Balance and Efficiency of the Pulsed Plasma Thruster," AIAA Paper 98-3808, 1988.

[9]Ishii, Y., Takagi, H., Yamamoto, T., and Tahara, H.," Flowfield Calculation of Electrothermal Pulsed Plasma Thrusters onboard the Osaka Institute of Technology Small Satellite," *27th International Symposium on Space Technology and Science*, Paper ISTS 2009-b-15, 2009.

[10]Edamitsu, T., Tahara, H., and Yoshikawa, T.," Performance Measurement and Flowfield Calculation of a Pulsed Plasma Thruster with a PTFE Cavity," *Asian Joint Conference on Propulsion and Power 2005*, Paper AJCPP2005-22083, 2005.

[11]Edamitsu, T., and Tahara, H.," Performance Measurement and Flowfield Calculation of an Electrothermal Pulsed Plasma Thruster with a Propellant Feeding Mechanism," *29th International Electric Propulsion Conference*, Paper IEPC-05-105, 2005.

[12]Edamitsu, T., and Tahara, H.," Experimental and Numerical Study of an Electrothermal Pulsed Plasma Thruster for Small Satellite," *Vacuum*, Vol.80, 2006, pp.1223-1228.

[13]Keider, M., Boyd, I.D., and Beilis, I.I.,," Model of an Electrothermal Pulsed Plasma Thruster," *IEEE Transactions on Plasma Science*, Vol.28, No.2, 2000, pp.376-385.

[14]Goodman, F.O., and Wachman, H.Y.," Formula for Thermal Accommodation Coefficients," *Journal of Chemical Physics*, Vol.46, No.6, 1967, pp.2376-2386.

[15]Langmuir, I.," The Evaporation, Condensation and Reflection of Molecules and the Mechanism of Adsorption," *Physical Review*, Vol.VIII, No.2, 1916.